

Locally adaptive total variation for removing mixed Gaussian-impulse noise

A. Langer^a

^a University of Stuttgart, Pfaffenwaldring 57, 70569 Stuttgart, Germany

ARTICLE HISTORY

Compiled February 5, 2018

ABSTRACT

The minimization of a functional consisting of a combined L^1/L^2 data fidelity term and a total variation regularization term with a locally varying regularization parameter for the removal of mixed Gaussian - impulse noise is considered. Based on a related locally constrained optimization problem, algorithms for automatically selecting the spatially varying parameter are presented. Numerical experiments for image denoising are shown, which demonstrate that the locally varying parameter selection algorithms are able to generate solutions which are of higher restoration quality than solutions obtained with scalar parameters.

KEYWORDS

Locally dependent regularization parameter; Automated parameter selection; Mixed Gaussian - impulse noise; Combined L^1/L^2 data fidelity; Total variation minimization

1. Introduction

Due to several reasons observed images are often contaminated by different types of noise and may be additionally distorted by some measurement device. In this paper we consider images which are containing a mixture of Gaussian and impulse noise, where we assume that first Gaussian noise and then impulse noise is added to the image. This might be, for example, the case if in the process of image acquisition Gaussian noise occurs and later while image transmission impulse noise is added. In this setting an observation g might be modeled as

$$\begin{cases} \bar{g} = T\hat{u} + \eta \\ g = \mathcal{N}(\bar{g}), \end{cases}$$

where \hat{u} is the unknown original image, T is a linear bounded operator modeling the image formation device, η is oscillatory with zero mean and standard deviation σ representing Gaussian white noise, and \mathcal{N} represents impulse noise. In most of the applications impulse noise is either modeled as salt-and-pepper or random-valued impulse noise. Assume that \bar{g} lies in the dynamic range $[d_{\min}, d_{\max}]$, i.e., $d_{\min} \leq \bar{g} \leq d_{\max}$.

Email: andreas.langer@mathematik.uni-stuttgart.de

d_{\max} almost everywhere. Then in the case of salt-and-pepper noise

$$g(x) = \begin{cases} d_{\min} & \text{with probability } s \\ d_{\max} & \text{with probability } s \\ \bar{g}(x) & \text{with probability } 1 - 2s \end{cases}$$

where $s \in [0, 1/2)$, and in the case of random valued impulse noise

$$g(x) = \begin{cases} \rho & \text{with probability } r \in [0, 1) \\ \bar{g}(x) & \text{with probability } 1 - r, \end{cases}$$

where ρ is a uniformly distributed random variable in the image intensity range $[d_{\min}, d_{\max}]$; see for example [7]. Note, that if first impulse noise and then Gaussian noise is added, a different observation is formed; see [28].

There exists a variety of different approaches for removing mixed Gaussian-impulse noise which usually start by estimating or detecting outliers (impulse noise) in the image and then adapt or use a Gaussian noise removal strategy; see for example [7, 16, 26, 32, 37, 41, 43]. In general, algorithms for Gaussian plus impulse noise removal may be classified in the following way: filter approaches [15, 36, 43], regularization based approaches [7, 13, 16, 26, 32, 38, 41, 42], Bayesian-based approaches [35], and patch-based approaches [12, 29, 33]. In this paper we consider a pure regularization approach by minimizing a functional consisting of a combined L^1 - L^2 -data-fidelity term and a total variation regularization term, introduced in [20]. It has been demonstrated that this optimization problem is suited to the task of removing mixed Gaussian-impulse noise; see [20, 28]. In this approach, which we call L^1 - L^2 -TV model, an image is restored by solving

$$\min_{u \in BV(\Omega)} \alpha_1 \|T_1 u - g_1\|_{L^1(\Omega)} + \alpha_2 \|T_2 u - g_2\|_{L^2(\Omega)}^2 + \lambda \int_{\Omega} |Du|, \quad (1)$$

where $\Omega \subset \mathbb{R}^2$ is an open bounded domain with Lipschitz boundary, $T_i : L^2(\Omega) \rightarrow L^2(\Omega)$ is a bounded linear operator, $g_i \in L^2(\Omega)$ is a given datum, $\alpha_i \geq 0$ for $i = 1, 2$ with $\alpha_1 + \alpha_2 > 0$, and $\lambda > 0$. Here, $\int_{\Omega} |Du|$ denotes the total variation (TV) of u in Ω ; see [3, 18] for more details. We note, that one parameter in (1) can be actually omitted. However, for good reasons, which will be clear later, we would like to keep the L^1 - L^2 -TV model in this form.

For removing a mixture of Gaussian and impulse noise from a single image g one typically sets $T_1 = T_2$ and $g_1 = g_2 = g$ in (1). In this setting it is easy to see that the L^1 - L^2 -TV model (1) is a generalization of the L^1 -TV model (if $\alpha_2 = 0$) and the L^2 -TV model (if $\alpha_1 = 0$). Modifications of the L^1 - L^2 -TV model have been presented in [19], where the total variation is replaced by $\|Wu\|_1$ with W being a wavelet tight frame transform, and in [34], where the second order total generalized variation [6] has been used as regularization term and box-constraints, which assure that the reconstruction lies in the respective dynamic range, are incorporated. It is worth to mention, that very recently in [8] a different regularization approach using an infimal convolution data fidelity term is proposed for mixed noise removal.

The minimizer of the L^1 - L^2 -TV model highly depends on the proper choice of α_i , $i = 1, 2$ and λ . In particular, if α_1 and α_2 are small compared to λ , then an over-smoothed reconstruction is obtained, which not only removes noise but also eliminates

details in the image. On the contrary, if α_1 and α_2 are large in comparison to λ , then the obtained solution fits the given data properly but retains noise. Note, that α_1 and α_2 additionally weight the importance of the L^1 -term and L^2 -term. In particular, we expect α_1 to be large if the noise in the image is impulse noise dominated, while for Gaussian noise dominated images α_2 should be sufficiently large. Hence for fixed λ a good reconstruction can be achieved by choosing α_1 and α_2 such that a good compromise of the aforementioned effects are made. For $\lambda = 1$ in [34] it is suggested to select the parameters according to the variance σ^2 of the Gaussian noise and the energy of the impulse noise, i.e.,

$$\alpha_1 = \frac{E_I}{E_I + \sigma^2} \quad \text{and} \quad \alpha_2 = \frac{\sigma^2}{E_I + \sigma^2}, \quad (2)$$

where $E_I = s$ for salt-and-pepper noise and $E_I = \frac{r}{3}$ for random-valued impulse noise. This parameter choice rule is used in [28] as an initial guess for an automated parameter selection algorithm, which is demonstrated to optimize the parameters further with respect to image quality measures. We emphasize, that the parameter selection algorithm of [28] chooses only scalar parameters.

Note, that images usually consist of large uniform regions as well as parts with fine details. Hence, scalar regularization parameters might not be the best choice; see [14, 27]. In particular, it is shown for the L^1 -TV and L^2 -TV model, that with a spatially varying weight better reconstructions (in the sense of certain quality measures) than with a globally constant parameter can be obtained, see for example [14, 25, 27]. We expect a similar behavior of the L^1 - L^2 -TV model. In this vein, in order to enhance image details while removing noise considerably in uniform regions we consider the minimization problem

$$\min_{u \in BV(\Omega)} \alpha_1 \|T_1 u - g_1\|_{L^1(\Omega)} + \alpha_2 \|T_2 u - g_2\|_{L^2(\Omega)}^2 + \int_{\Omega} \lambda(x) |Du|, \quad (3)$$

where $\lambda : \Omega \rightarrow \mathbb{R}^+$ is a function. In this paper we address the question, how to choose λ automatically in a suitable way.

Let us mention, that spatially varying choices of parameters for the L^2 -TV and L^1 -TV model are for example introduced in [2, 4, 9, 14, 17, 21, 23–25, 27, 31, 39]. Other data terms with locally varying parameters have for example been considered in [11, 30]. However, the combined L^1 - L^2 -TV model has not yet been considered with respect to spatially varying parameter choices. To the best of our knowledge, in this paper we present the first approach in this direction. In order to do so we utilize the locally adaptive parameter approach of [27], which is based on the discrepancy principle and developed solely for the L^2 -TV and L^1 -TV model, and adapt it to our model. In this vein we relate (3) to a locally constrained optimization problem, see (4) below. We consider two different approaches on how to choose the local bounds in the constituted constraints and compare them numerically by experiments.

The contribution of the present paper is two-sided: Firstly, we present the first attempt of choosing a spatially adaptive parameter in the L^1 - L^2 -TV model. Secondly, we compare two different approaches on how to choose the local bounds. In particular, this allows us to show the full strength of a locally varying parameter and shows at the same time the importance of properly chosen local bounds.

1.1. Locally constrained minimization problem

In order to obtain a suitable λ in (3), we formulate, as in [14, 25, 27], a locally constrained optimization problem in the following way:

$$\min_{u \in BV(\Omega)} \int_{\Omega} |Du| \quad \text{subject to (s.t.)} \quad \mathcal{S}(u) \leq \mathcal{B} \quad \text{almost everywhere (a.e.) in } \Omega, \quad (4)$$

where $\mathcal{S}(u)(\cdot) := \int_{\Omega} w(\cdot, y) \mathcal{H}(u)(y) dy$ with w being a normalized localization filter, i.e., $w \in L^{\infty}(\Omega \times \Omega)$, and $w \geq 0$ on $\Omega \times \Omega$ with

$$\begin{aligned} & \int_{\Omega} \int_{\Omega} w(x, y) dy dx = 1, \\ & \int_{\Omega} \int_{\Omega} w(x, y) |\phi|(y) dy dx \geq \epsilon \|\phi\|_{L^1(\Omega)} \quad \text{for all } \phi \in L^1(\Omega) \quad \text{and} \\ & \int_{\Omega} \int_{\Omega} w(x, y) \phi^2(y) dy dx \geq \epsilon \|\phi\|_{L^2(\Omega)}^2 \quad \text{for all } \phi \in L^2(\Omega) \end{aligned} \quad (5)$$

for some $\epsilon > 0$ independent of ϕ , cf. [25], and $\mathcal{H}(u)(y) := \alpha_1 |T_1 u - g_1|(y) + \alpha_2 |T_2 u - g_2|^2(y)$. Here, $\mathcal{B} \in \mathbb{R}$ is some value depending on the type of noise. Although the value \mathcal{B} is here a fixed constant, in our numerical experiments we report on results where \mathcal{B} is chosen empirically based on some approximation of the true image. Moreover, we define the feasible set

$$U := \{u \in BV(\Omega) : \mathcal{S}(u) \leq \mathcal{B} \text{ a.e. in } \Omega\}.$$

A function w which satisfies the conditions in (5) is, for instance, the mean filter defined as

$$w(x, y) := \begin{cases} \frac{1}{\omega_{\delta}} & \text{if } |y - x|_{\ell^{\infty}} \leq \frac{\omega}{2}, \\ \delta & \text{otherwise,} \end{cases}$$

with $x \in \Omega$ being fixed, $\omega > 0$ sufficiently small (representing the essential width of the filter window), $0 < \delta \ll 1$ and ω_{δ} chosen such that $\int_{\Omega} \int_{\Omega} w(x, y) dy dx = 1$; see [14, 25].

Next, we are going to show the existence of minimizers of (4) by using the following lemma.

Lemma 1.1. *Let $\mathcal{Q}(u) = \mathcal{R}(u) + \int_{\Omega} \mathcal{S}(u)(x) dx$. Assume there exist $i \in \{1, 2\}$ such that T_i does not annihilate constant functions, i.e., $T_i \chi_{\Omega} \neq 0$, where $\chi_{\Omega}(x) = 1$ if $x \in \Omega$. Then $\|u\|_{BV} \rightarrow \infty$ implies $\mathcal{Q}(u) \rightarrow \infty$.*

By noting that the conditions in (5) hold, the proof of this lemma follows the lines of the proof of [28, Lemma 3.1].

Theorem 1.2. *Assume there exist $i \in \{1, 2\}$ such that T_i does not annihilate constant functions and $U \neq \emptyset$. Then the problem in (4) has a solution $u \in BV(\Omega)$.*

Using Lemma 1.1 the proof of this statement is analog to the proof of [14, Theorem 2] and [25, Theorem 2].

2. Locally adaptive algorithm

In what follows we consider a discrete image domain again denoted by Ω containing $N_1 \times N_2$ pixels, $N_1, N_2 \in \mathbb{N}$. The considered function spaces are $X \in \mathbb{R}^{N_1 \times N_2}$ and $Y = X \times X$. For $u \in X$ we use the following norms

$$\|u\|_{\ell^\tau(\Omega)}^\tau = \sum_{x \in \Omega} |u(x)|^\tau$$

for $\tau \in \{1, 2\}$. Then the discrete version of the functional in (3) writes as

$$J(u, \lambda) := \alpha_1 \|T_1 u - g_1\|_{\ell^1(\Omega)} + \alpha_2 \|T_2 u - g_2\|_{\ell^2(\Omega)}^2 + \sum_{x \in \Omega} \lambda(x) |\nabla u(x)|_{l^2} \quad (6)$$

where $|y|_{l^2} = \sqrt{y_1^2 + y_2^2}$ for every $y = (y_1, y_2)$, $\lambda : \Omega \rightarrow \mathbb{R}^+$ is a discrete function, $T_i : X \rightarrow X$ is a bounded linear operator, $g_i \in X$ is a given datum, and $\alpha_i \geq 0$ for $i = 1, 2$ with $\alpha_1 + \alpha_2 > 0$. Here and in the sequel ∇ represents the discrete gradient (discretized by using forward differences; cf. [10, 22]) and $\text{div} = -\nabla^T$. Moreover, we assume that T_i is diagonal for $i = 1, 2$, i.e., there exists $\tilde{T}_i \in X$ associated with T_i such that $T_i u = \tilde{T}_i \circ u$ (Hadamard product) with $[\tilde{T}_i \circ u](x) = \tilde{T}_i(x)u(x)$ for any $u \in X$ and $x \in \Omega$. This is for example the case when $T_i = I$ or $T_i = \chi_D$, where χ_D denotes the characteristic function of the domain $D \subset \Omega$, which are the two relevant cases for our numerical experiments.

2.1. The locally constrained problem

For a reasonable choice of λ in (6) we consider the following optimization problem with local constraints, cf. (4):

$$\min_{u \in X} \|\nabla u\|_{\ell^1(\Omega)} \quad \text{s.t.} \quad S(u)(x) \leq B \quad \text{for all } x \in \Omega, \quad (7)$$

where

$$S(u)(x) := \frac{1}{|\mathcal{I}(x)|} \sum_{y \in \mathcal{I}(x)} \sum_{\tau=1}^2 \alpha_\tau |(T_\tau u)(y) - g_\tau(y)|^\tau$$

denotes a kind of local residual at $x \in \Omega$ with $\mathcal{I}(x)$ being some suitable set of pixels around x of size $|\mathcal{I}(x)|$ (i.e. $|\mathcal{I}(x)|$ denotes the number of pixels in $\mathcal{I}(x)$) and $B \geq 0$ denotes the noise-level of the respective noise, which may depend on the true (unknown) image \hat{u} ; cf. (4). For more details on the choice of B we refer to Section 2.2 below.

In the sequel, as in [27], we set

$$\mathcal{I}(x) := \left\{ y \in \Omega : |x - y| \leq \frac{\omega - 1}{2} \right\},$$

that is, $\mathcal{I}(x) \subset \Omega$ for all $x \in \Omega$, and ω being an odd number determining the size. With this separation of the image domain we obtain the following results.

Proposition 2.1. *If u is a solution of (7), then we have that*

$$H(u) := \alpha_1 \|T_1 u - g_1\|_{\ell^1(\Omega)} + \alpha_2 \|T_2 u - g_2\|_{\ell^2(\Omega)}^2 \leq B|\Omega|.$$

Proof. Let u be a minimizer of (7), then we have that

$$\begin{aligned} B|\Omega| &= |\Omega|(\alpha_1 \nu_1 + \alpha_2 \nu_2) \geq \sum_{x \in \Omega} S(u)(x) = \sum_{x \in \Omega} \frac{1}{|\mathcal{I}(x)|} \sum_{y \in \mathcal{I}(x)} \sum_{\tau=1}^2 \alpha_\tau |(T_\tau u)(y) - g_\tau(y)|^\tau \\ &= \sum_{x \in \Omega} \sum_{\tau=1}^2 \alpha_\tau |(T_\tau u)(x) - g_\tau(x)|^\tau = \alpha_1 \|T_1 u - g_1\|_{\ell^1(\Omega)} + \alpha_2 \|T_2 u - g_2\|_{\ell^2(\Omega)}^2 \end{aligned}$$

where we used that, due to the sum over $x \in \Omega$ each picture element $y \in \mathcal{I}(x)$ occurs exactly $|\mathcal{I}(x)|$ -times. \square

From this proposition it follows that a minimizer of the locally constrained problem (7) also satisfies the constraint of the globally constrained problem

$$\min_{u \in X} \|\nabla u\|_{\ell^1(\Omega)} \quad \text{s.t.} \quad H(u) \leq B|\Omega| \quad (8)$$

but is in general of course not a solution of (8). Consequently, [27, Proposition 4.2] holds also in our framework, which we recall next for completeness.

Proposition 2.2. *Let u_s and u_l be solutions of (8) and (7) respectively. Then we have that*

$$\|\nabla u_s\|_{\ell^1(\Omega)} \leq \|\nabla u_l\|_{\ell^1(\Omega)}.$$

This statement says that the total variation of the solution of (7) cannot be smaller than the total variation of the minimizer of (8). Meaning that the locally constrained problem is expected to preserve more details than the globally constrained problem. However, we keep in mind that noise may be interpreted as fine details.

2.2. On the choice of the local bounds

In this paper we consider two different approaches of choosing the local bounds B , which we are going to compare numerically in Section 3.

2.2.1. Approach 1

Assume that for an image corrupted by mixed Gaussian-impulse noise the probability s or r , depending which type of impulse noise (i.e., salt-and-pepper or random-valued impulse noise) is present in the image, and the standard deviation σ of Gaussian noise is at hand. Then the expected absolute value (EAV) ν_1 and the variance ν_2 of the mixed Gaussian-impulse noise can be estimated as in [28]. More precisely, knowing s, r and σ allows us to compute the EAV of each single present noise type. Then ν_1 is the sum of the EAV of the impulse noise and Gaussian noise and ν_2 is the sum of the variances of both noises. Then the local bound B is set to $B = \alpha_1 \nu_1 + \alpha_2 \nu_2$. The

motivation of the above choice of B is, that we wish for a restoration u such that

$$\|T_1 u - g_1\|_{\ell^1(\mathcal{I}(x))} \leq \nu_1 |\mathcal{I}(x)| \quad \text{and} \quad \|T_2 u - g_2\|_{\ell^2(\mathcal{I}(x))}^2 \leq \nu_2 |\mathcal{I}(x)| \quad (9)$$

and hence $\|T_1 u - g_1\|_{\ell^1(\mathcal{I}(x))} + \|T_2 u - g_2\|_{\ell^2(\mathcal{I}(x))}^2 \leq (\nu_1 + \nu_2) |\mathcal{I}(x)|$. We are aware, that a solution of (7) in general does not fulfill the inequalities in (9). However, we expect for a minimizer of (7), that these inequalities are at least not too much violated. This expectation is based on the fact, that if a solution of (7) violates one of the inequalities in (9) the other inequality holds automatically. Further, if $T_1 = T_2$ and $g_1 = g_2$, which is the typical setting for restoring a single image, then this fact is additionally accompanied by the circumstance, that the ℓ^1 -norm and the squared ℓ^2 -norm behave similarly (they are both convex and share the same minimum). That is, if one of these norms is increasing the other does as well.

As one sees from the calculation in [28], ν_1 and ν_2 may depend on the original image \hat{u} . Whenever this happens for at least one ν_τ , $\tau \in \{1, 2\}$, problem (7) results in a quite non-linear problem, since B becomes $B(u)$. Instead of considering non-linear constraints we choose a reference image \tilde{u} and compute an approximation $B = B(\tilde{u})$. Since our proposed algorithms are of iterative nature (see LATV- and pLATV-algorithm below), the reference image \tilde{u} is chosen as the current approximation (see LATV- and pLATV-algorithm below). Then, with this new value B we are solving (7).

2.2.2. Approach 2

We suppose that we know in each window $\mathcal{I}(x)$, $x \in \Omega$, the true expected absolute value and standard deviation of the mixed noise. Then (7) writes as

$$\min_{u \in X} \|\nabla u\|_{\ell^1(\Omega)} \quad \text{s.t.} \quad S(u)(x) \leq B(x) \quad \text{for all } x \in \Omega, \quad (10)$$

where $B(x) = c(\alpha_1 \nu_1(x) + \alpha_2 \nu_2(x))$ with $\nu_1(x)$ and $\nu_2(x)$ being the known EAV and standard deviation in $\mathcal{I}(x)$ for $x \in \Omega$ and $c > 0$ is a constant experimentally obtained. In particular in our numerics it turns out that $c = 0.95$ does a good job for all considered examples and hence we set it exactly to that value for all our experiments.

Similar to Proposition 2.1 we can show that a minimizer of (10) satisfies the condition of the globally constrained problem

$$\min_{u \in X} \|\nabla u\|_{\ell^1(\Omega)} \quad \text{s.t.} \quad H(u) \leq \sum_{x \in \Omega} B(x).$$

Note, that $\sum_{x \in \Omega} B(x) = B|\Omega|$ if $B(x) =: B$ is constant for all $x \in \Omega$.

We summarize that the main difference between approach 1 and approach 2 is, that in approach 1 the bound B is constant in whole Ω , while for approach 2 it is spatially varying.

Our numerical experiments demonstrate that approach 2 is superior to approach 1. However, obtaining the exact values $\nu_1(x)$ and $\nu_2(x)$ for any $x \in \Omega$ seems very challenging and is not part of the present paper, but will be considered in future research.

In the sequel, in order to keep the paper concise, we will write $B(x)$ or $B(\tilde{u})(x)$ independently whether the bound is constant for any $x \in \Omega$ or not.

2.3. Local parameter selection

Note, that for small $\alpha_1, \alpha_2 > 0$ (small compared to λ) the minimization of (1) yields an over-smoothed restoration u_{α_1, α_2} and we expect $H(u_{\alpha_1, \alpha_2}) > \sum_{x \in \Omega} B(x)$. Similar, if $S(u)(x) > B(x)$ we suppose that this is because u is over-smoothed in $\mathcal{I}(x)$ and hence we intend to decrease λ in the local region $\mathcal{I}(x)$. By similar considerations as in [27] we obtain the following locally adapted algorithm:

Algorithm 1 (LATV-Algorithm). Initialize $p := p_0 > 0$, $\lambda_0 > 0$ and set $n = 0$;

- 1) Compute $u_{\lambda_n} \in \arg \min_{u \in X} J(u, \lambda_n)$
- 2) (a) If $H(u_{\lambda_0}) > \sum_{x \in \Omega} B(u_{\lambda_0})(x)$, then set

$$f(x) := \max \{S(u_{\lambda_n})(x), B(u_{\lambda_n})(x)\}$$

- (b) If $H(u_{\lambda_0}) < \sum_{x \in \Omega} B(u_{\lambda_0})(x)$, then set

$$f(x) := \max \{\min \{S(u_{\lambda_n})(x), B(u_{\lambda_n})(x)\}, \varepsilon\}$$

- 3) Update

$$\lambda_{n+1}(x) := \frac{\lambda_n(x)}{|\mathcal{I}(x)|} \sum_{y \in \mathcal{I}(x)} \left(\frac{B(u_{\lambda_n})(y)}{f(y)} \right)^p \quad \text{for all } x \in \Omega.$$

- 4) Stop or set $n := n + 1$ and return to step 1).

In order to ensure that $f(x) > 0$ for all $x \in \Omega$ in every iteration, we introduce the small constant $\varepsilon > 0$, e.g., we set $\varepsilon = 10^{-14}$ in our experiments.

If $H(u_{\lambda_0}) > \sum_{x \in \Omega} B(u_{\lambda_0})(x)$, we terminate the algorithm as soon as the residual $H(u_{\lambda_n}) < \sum_{x \in \Omega} B(u_{\lambda_n})(x)$ for the first time and set the desired locally varying $\lambda^* = \lambda_n$. If $H(u_{\lambda_0}) < \sum_{x \in \Omega} B(u_{\lambda_0})(x)$, we stop the algorithm as soon as the residual $H(u_{\lambda_n}) > \sum_{x \in \Omega} B(u_{\lambda_n})(x)$ for the first time and set the desired locally varying $\lambda^* = \lambda_{n-1}$, since $H(u_{\lambda_{n-1}}) \leq \sum_{x \in \Omega} B(u_{\lambda_{n-1}})(x)$.

From [27] we have the following monotonicity property.

Proposition 2.3 ([27, Proposition 4.4]). *The LATV-algorithm generates a sequence $(\lambda_n)_n$ such that $(\sum_{x \in \Omega} \lambda_n(x))_n$ is monotone.*

Similar as in [27] the power p might be chosen adaptively leading to the following algorithm:

Algorithm 2 (pLATV-Algorithm). Initialize $p := p_0 > 0$, $\lambda_0 > 0$ and set $n = 0$;

- 1) Compute $u_{\lambda_0} \in \arg \min_{u \in X} J(u, \lambda_0)$
- 2) (a) If $H(u_{\lambda_0}) > \sum_{x \in \Omega} B(u_{\lambda_0})(x)$, then set

$$f(x) := \max \{S(u_{\lambda_n})(x), B(u_{\lambda_n})(x)\}.$$

- (b) If $H(u_{\lambda_0}) < \sum_{x \in \Omega} B(u_{\lambda_0})(x)$, then set

$$f(x) := \max \{\min \{S(u_{\lambda_n})(x), B(u_{\lambda_n})(x)\}, \varepsilon\}.$$

- 3) Update

$$\lambda_{n+1}(x) := \frac{\lambda_n(x)}{|\mathcal{I}(x)|} \sum_{y \in \mathcal{I}(x)} \left(\frac{B(u_{\lambda_n})(y)}{f(y)} \right)^p \quad \text{for all } x \in \Omega.$$

- 4) Compute $u_{\lambda_{n+1}} \in \arg \min_{u \in X} J(u, \lambda_{n+1})$
- 5) (a) if $H(u_{\lambda_0}) > \sum_{x \in \Omega} B(u_{\lambda_0})(x)$
 - (i) if $H(u_{\lambda_{n+1}}) \geq \sum_{x \in \Omega} B(u_{\lambda_{n+1}})(x)$, go to step 6)
 - (ii) if $H(u_{\lambda_{n+1}}) < \sum_{x \in \Omega} B(u_{\lambda_{n+1}})(x)$, decrease p , e.g., set $p = p/10$, and go to step 2)
- (b) if $H(u_{\lambda_0}) \leq \sum_{x \in \Omega} B(u_{\lambda_0})(x)$
 - (i) if $H(u_{\lambda_{n+1}}) \leq \sum_{x \in \Omega} B(u_{\lambda_{n+1}})(x)$, go to step 6)
 - (ii) if $H(u_{\lambda_{n+1}}) > \sum_{x \in \Omega} B(u_{\lambda_{n+1}})(x)$, decrease p , e.g., set $p = p/10$, and go to step 2)
- 6) Stop or set $n := n + 1$ and return to step 2).

This algorithm is terminated as soon as $|H(u_{\lambda_n}) - \sum_{x \in \Omega} B(u_{\lambda_n})(x)| \leq 10^{-6}$ and $H(u_{\lambda_n}) \leq \sum_{x \in \Omega} B(u_{\lambda_n})(x)$ for the first time. Additionally we stop iterating when p is less than machine precision, since then anyway no progress is to expect. Due to the adaptive choice of p we obtain a monotonic behavior of the sequence $(\lambda_n)_n$; see [27, Proposition 4.5].

Note, that the LATV- and pLATV-algorithm do not adjust the parameters α_1 and α_2 , which are weighting the importance of the L^1 - and L^2 -norm. In particular, as already mentioned above, we would like to choose α_1 large if the noise in the image is impulse noise dominated, while for Gaussian noise dominated images α_2 should be sufficiently large. In order to use suitable α_1 and α_2 we set them according to (2).

The LATV- and pLATV-algorithm only allows that $\lambda_n(x)$ for all x is either not increased or not decreased. That is, it is not possible that $\lambda_n(x_1)$ is increased and $\lambda_n(x_2)$ is decreased for arbitrary $x_1, x_2 \in \Omega$. Hence the initial value λ_0 has to be chosen sufficiently large or sufficiently small. In our experiments $\lambda_0 = 1$ owns this property.

2.4. Primal-dual algorithm for locally adaptive total variation

Since T_i , $i = 1, 2$, is diagonal, a minimizer of problem (3) is computed by utilizing the primal-dual approach proposed by Chambolle and Pock [10], which is already used for approximating a solution of the (scalar) L^1 - L^2 -TV problem (1) in [1] in a finite element setting. For $T_1 = T_2 = I$ the steepest descent algorithm runs as follows:

Algorithm 3 (Primal-dual algorithm). Initialize $\tau, \rho > 0$, $\theta \in [0, 1]$, $\vec{p}_0 \in Y$, $u_0 = \bar{u}_0 \in X$ and set $n = 0$;

- 1) Update $\vec{p}_{k+1}(x) = \frac{\vec{p}_k(x) + \sigma \nabla \bar{u}(x)}{\max\{\frac{1}{\lambda(x)}|\vec{p}_k(x) + \sigma \nabla \bar{u}(x)|, 1\}}$
- 2) Update

$$u_{k+1}(x) = \begin{cases} z(x) - \beta & \text{if } z(x) - \beta > g_1(x), \\ z(x) + \beta & \text{if } z(x) + \beta < g_1(x), \\ g_1(x) & \text{else ,} \end{cases}$$

where $z = \frac{1}{1+2\tau\alpha_2}(u_k + \tau \operatorname{div} \vec{p}_{k+1} + 2\tau\alpha_2 g_2)$ and $\beta = \frac{\tau\alpha_1}{1+2\tau\alpha_2}$.

- 3) Update $\bar{u}_{k+1} = u_{k+1} + \theta(u_{k+1} - u_k)$.
- 4) Stop or set $k := k + 1$ and return to step 1).

If $\theta = 1$ and $\tau\sigma\|\nabla\|^2 < 1$, then the convergence of this iterative scheme is ensured; see [10].

For $T_1 = \chi_{\Omega_1}$ and $T_2 = \chi_{\Omega_2}$, which is the case in the example considered in section 3.3, where $\Omega_1, \Omega_2 \subseteq \Omega$, then we still use Algorithm 3 by just replacing in step 2 z and β with $z(x) = \frac{1}{1+2\tau\alpha_2\chi_{\Omega_2}(x)}(u_k(x) + \tau \operatorname{div} \vec{p}_{k+1}(x) + 2\tau\alpha_2\chi_{\Omega_2}(x)g_2(x))$ and $\beta(x) = \frac{\tau\chi_{\Omega_1}(x)\alpha_1}{1+2\tau\chi_{\Omega_2}(x)\alpha_2}$ for all $x \in \Omega$, respectively.

3. Numerical results

In the following we present numerical experiments for studying the behavior of the proposed algorithms (i.e., LATV- and pLATV-algorithm) with respect to its image restoration capabilities. We consider the LATV- and pLATV-algorithm with both types of local bounds described in Section 2.2 to which we will refer as approach 1 and approach 2.

The performance of these methods is compared quantitatively by means of peak signal-to-noise ratio (PSNR) [5], which is widely used as an image quality assessment measure and the mean structural similarity measure (MSSIM) [40], which relates to perceived visual quality better than PSNR. In general, when comparing PSNR and MSSIM, large values indicate better reconstruction than smaller values.

For our numerical studies we consider the images shown in Figure 1 of size 256×256 pixels. The image intensity range of these images is scaled to $[0, 1]$.

In all our experiments the initial power p is chosen to be $\frac{1}{2}$ and $\lambda_0 = 1$. Moreover, the parameters α_1 and α_2 are chosen according to (2). The optimization problem occurring in step 1 of the LATV-algorithm and in step 1 and step 4 of the pLATV-algorithm are solved via the primal-dual scheme in Algorithm 3. For the primal-dual algorithm we set $\theta = 1$ and $\sigma = \tau = (0.9/8)^{1/2}$. Since we are using the discretization used in [10] with spacing-size 1, $\|\nabla\|^2 = 8$ and hence $\tau\sigma\|\nabla\|^2 < 1$, which ensures the convergence of the used primal-dual algorithm. This algorithm is terminated as soon as the relative

differences of two successive iterates are smaller than a certain tolerance, i.e., in our experiments as soon as

$$\frac{\|\vec{p}_k - \vec{p}_{k-1}\|_{\ell^1}}{\|\vec{p}_k\|_{\ell^1}} \leq 10^{-4} \quad \text{and} \quad \frac{\|u_k - u_{k-1}\|_{\ell^1}}{\|u_k\|_{\ell^1}} \leq 10^{-4}$$

for the first time.

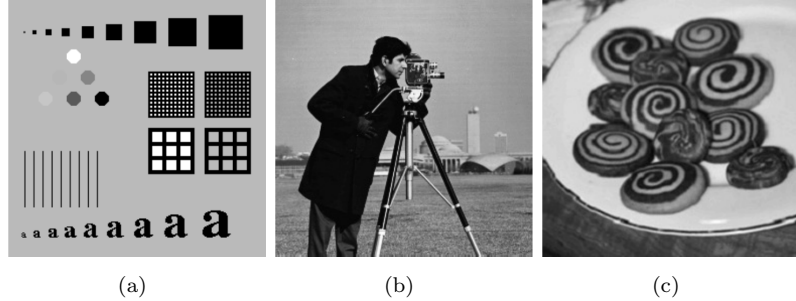


Figure 1. *Original images: (a) phantom (b) cameraman (c) cookies*

3.1. Dependency on the window-size

We test the influence of the window-size ω on the restorations obtained by the proposed LATV- and pLATV-algorithm. To do so, we consider the cookies-image, see Figure 1(c), distorted by different levels of mixed Gaussian and salt-and-pepper noise and we vary ω from 3 to 19. Figure 2 shows the PSNR and MSSIM of the respective restorations obtained via the LATV-algorithm and pLATV-algorithm using approach 1 while in Figure 3 we used approach 2. From these experiments we observe that larger window-sizes ω usually decrease the PSNR and MSSIM of the reconstructions, while for the LATV-algorithm using approach 1 we observe exactly the opposite behavior. Similar observations are made for other images as well, e.g., the cameraman-image from Figure 1(b). This indicates to use a large window-size (e.g. $\omega = 19$) in the LATV-algorithm with approach 1 and a very small window-size (e.g., $\omega = 3$) for all the other cases.

In Figure 2 and Figure 3 we also indicate the number of iterations needed till termination, which shows that the pLATV-algorithm needs a massive amount of more iterations than the LATV-algorithm. Moreover we observe that for the LATV-algorithm the number of iteration are increasing with increasing ω , while this is in general not the case for the pLATV-algorithm, which anyway needs much more iterations till termination, due to the adaptivity of p .

3.2. Comparison with scalar parameter

Now we compare the performance of the LATV- and pLATV-algorithm with two scalar parameter choice approaches. The first one is the algorithm proposed in [28], which automatically selects the scalar parameters α_1 and α_2 in (1) with $\lambda = 1$. In the sequel we refer to this algorithm as the α_1 - α_2 -pAPS. Note, that in this strategy the initial α_1 and α_2 are computed according to (2). As the second scalar parameter selection method we utilize the approach presented in [27] for automatically computing scalar

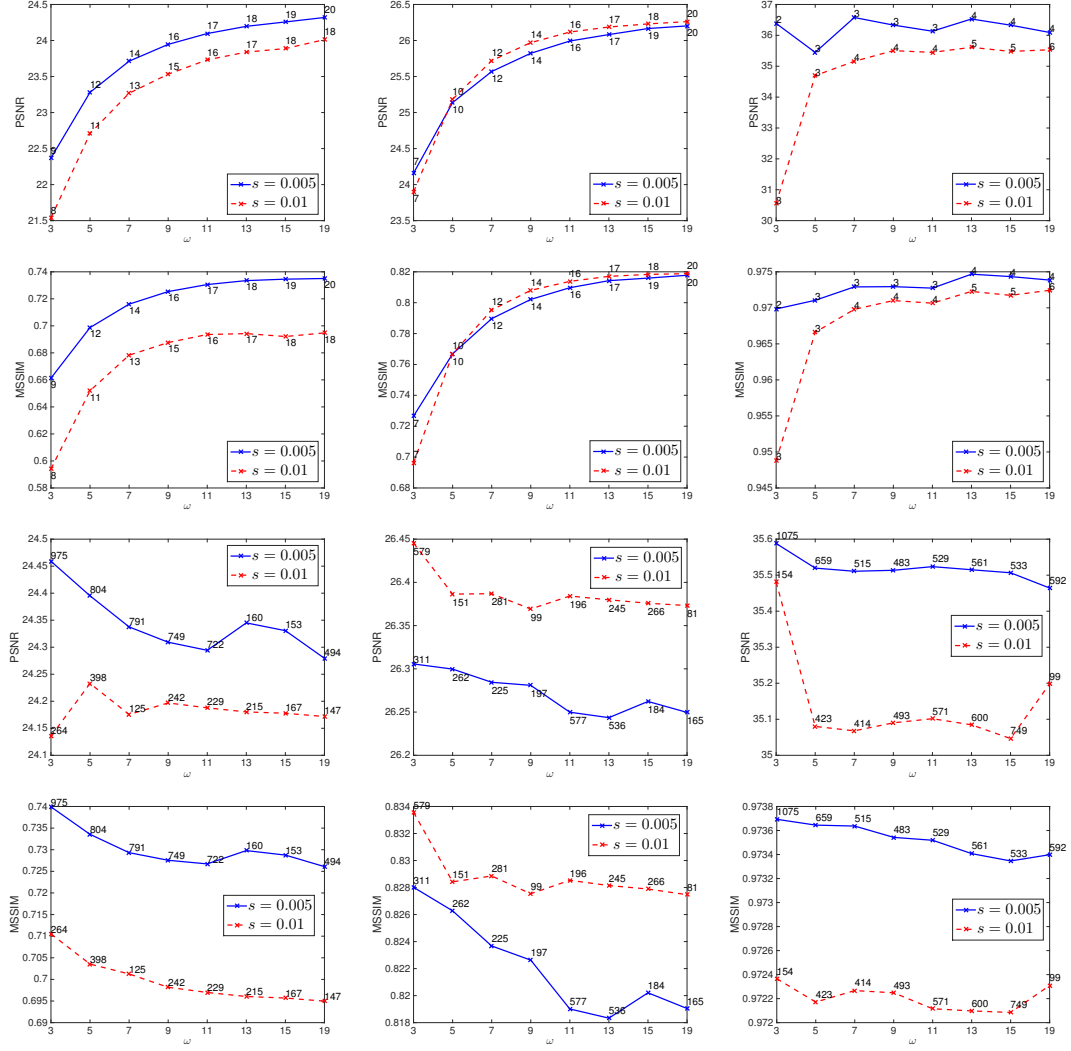


Figure 2. Restoration via the LATV-algorithm (first two rows) and via the pLATV-algorithm (last two rows) of the cookies-image corrupted with Gaussian white noise with $\sigma = \sqrt{0.02}$ (left column), $\sigma = 0.1$ (middle column), $\sigma = 0.01$ (right column) and salt-and-pepper noise.

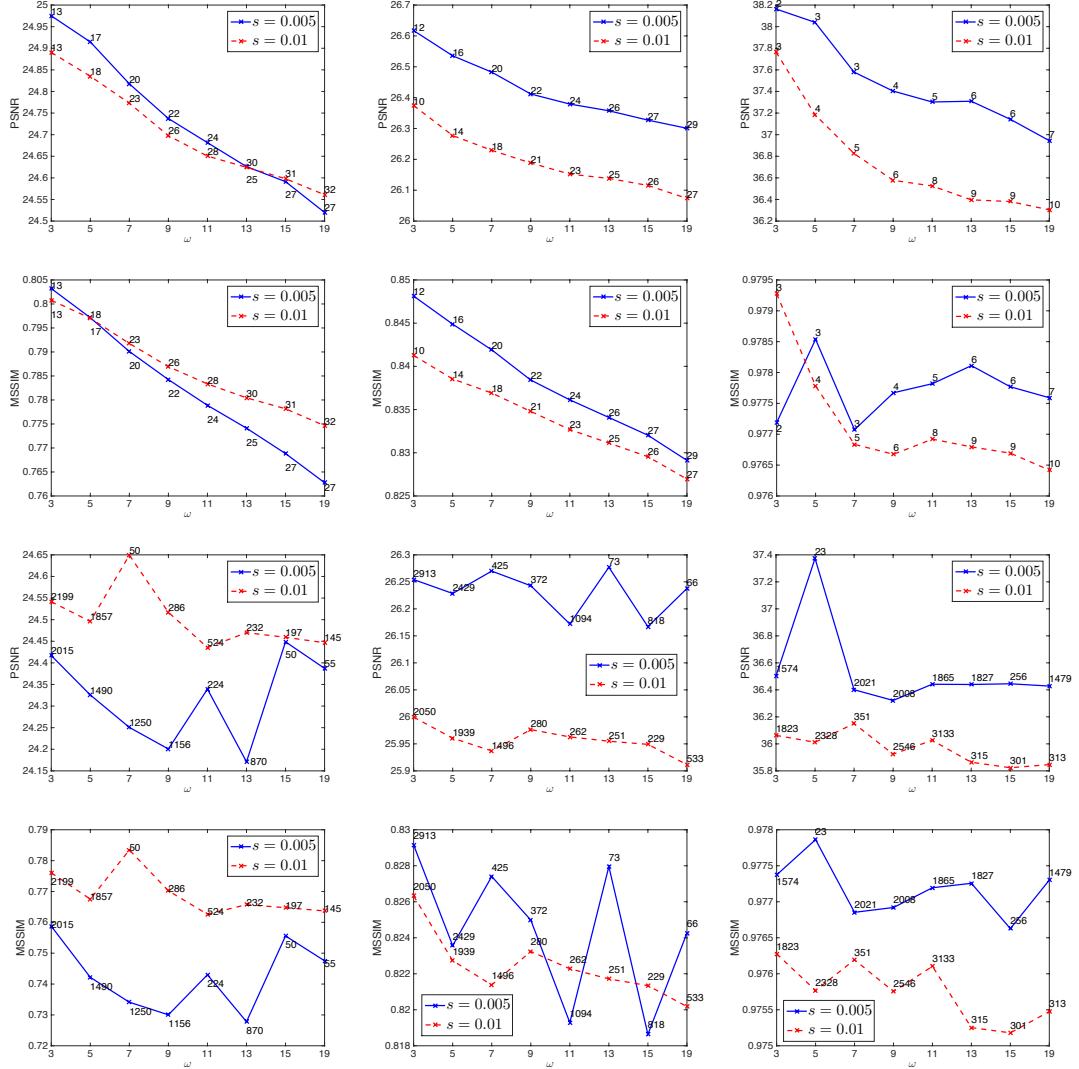


Figure 3. Restoration via the LATV-algorithm (first two rows) and via the pLATV-algorithm (last two rows) using approach 2 of the cookies-image corrupted with Gaussian white noise with $\sigma = \sqrt{0.02}$ (left column), $\sigma = 0.1$ (middle column), $\sigma = 0.01$ (right column) and salt-and-pepper noise.

λ 's whereby α_1 and α_2 are fixed and chosen according to (2). We refer to it as the λ -pAPS. In this approach we relate (1) to the constrained optimization problem

$$\min_{u \in BV(\Omega)} \int_{\Omega} |Du| \quad \text{s.t.} \quad \frac{1}{|\Omega|} \mathcal{H}(u) = \mathcal{B}$$

where $\mathcal{H}(u) := \alpha_1 \|T_1 u - g_1\|_{L^1(\Omega)} + \alpha_2 \|T_2 u - g_2\|_{L^2(\Omega)}^2$, $\mathcal{B} = \alpha_1 \nu_1 + \alpha_2 \nu_2$ is a constant depending on the noise, and $|\Omega|$ denotes the volume of Ω . Then the so-called pAPS-algorithm proposed in [27] is utilized to compute suitable parameters λ .

For our comparison we distort the original images shown in Figure 1 with mixed Gaussian-impulse noise with different noise-levels, i.e., $\sigma = \{\sqrt{0.02}, 0.1, 0.01\}$, $s = \{0.01, 0.005\}$, and $r = \{0.01, 0.005\}$, and restore them with the above mentioned algorithms. Our findings are summarized in Table 1 and Table 2 for Gaussian plus salt-and-pepper noise removal and in Table 3 and Table 4 for eliminating mixed Gaussian - random-valued noise. From these tables we observe that the LATV- and pLATV-algorithm using approach 2 for the local bounds outperform (with respect to the quality measures PSNR and MSSIM) the scalar parameter selection strategies in all considered experiments. This is slightly different for using approach 1 in the LATV- and pLATV-algorithm. While for removing Gaussian + random-valued noise these algorithms still give better results in all experiments than the scalar parameter methods, this is not always the case for the simultaneous removal of Gaussian and salt-and-pepper noise. In the latter case in a few cases the scalar parameter algorithms generate results with larger PSNR and MSSIM.

From all these experiments we observe that the LATV-algorithm using approach 2 for the local bounds seems to give always the results with the largest PSNR and MSSIM. This clearly indicates that the choice of the local bounds are very crucial in order to utilize the strength of locally adaptive parameters. The strength of these approaches is also visible in Figure 4 - 8, where we depict for certain noise-levels the generated reconstruction of the corresponding algorithm. For example in Figure 4 we observe that the scalar parameter choice methods are not able to preserve all features. There, e.g., the bars in the left upper part are partly vanished. On the contrary, the locally adaptive parameter choice methods are able to retain these features much better. In particular, the LATV-algorithm with approach 2 gives the visually best results, which is also affirmed by the largest PSNR and MSSIM. The presented figures show, that the reconstructions of the locally adaptive algorithms depend on the local bounds and that they are able to generate visually much better results than scalar parameter methods.

3.3. Separated noise

Here we consider an example where salt-and-pepper noise and Gaussian noise is disjoint present in an image. More precisely, we consider the image in Figure 9(a) where the lower half g_1 is contaminated only with salt-and-pepper noise ($s = 0.1$) and in the upper half g_2 only Gaussian white noise ($\sigma = 0.1$) is contained. That is, in this situation $g_1 \neq g_2$. The associated image domains are Ω_1 and Ω_2 , which are two disjoint subdomains of Ω such that $\Omega_1 = \Omega \setminus \Omega_2$ and $\Omega = \Omega_1 \cup \Omega_2$. We are aware that this is a rather artificial example. However, it is very interesting from a numerical point of view, since a correct global solution cannot be obtained by just separating the image into an upper and a lower part due to the non-additivity of the total variation [20].

Table 1. Removal of Gaussian + salt-and-pepper noise.

image	σ	s	$\alpha_1\alpha_2$ -PAPS		λ -pAPS		LATV approach 1 with $\omega = 19$		pLATV approach 1 with $\omega = 3$	
			PSNR	MSSIM	PSNR	MSSIM	PSNR	MSSIM	PSNR	MSSIM
phantom	$\sqrt{0.02}$	0.005	22.32	0.7641	22.73	0.7730	23.53	0.8137	23.27	0.8044
		0.01	21.08	0.6752	21.84	0.6852	22.37	0.7211	22.00	0.6941
	0.1	0.005	23.99	0.8190	24.85	0.8348	26.01	0.8770	25.65	0.8670
		0.01	22.85	0.7479	24.63	0.7975	25.31	0.8388	25.27	0.8428
	0.01	0.005	28.14	0.9747	27.63	0.9704	31.61	0.9908	30.07	0.9868
		0.01	25.54	0.9555	25.23	0.9510	28.56	0.9854	27.69	0.9760
cameraman	$\sqrt{0.02}$	0.005	23.21	0.6252	24.33	0.6625	23.91	0.6683	23.92	0.6682
		0.01	22.38	0.5520	24.24	0.6181	23.22	0.5945	23.24	0.5894
	0.1	0.005	24.28	0.6652	26.00	0.7441	25.82	0.7542	25.77	0.7565
		0.01	23.80	0.6195	25.78	0.7223	25.84	0.7348	25.78	0.7217
	0.01	0.005	32.42	0.9385	32.41	0.9388	33.01	0.9468	32.57	0.9466
		0.01	31.36	0.9325	31.73	0.9342	32.01	0.9436	31.31	0.9419
cookies	$\sqrt{0.02}$	0.005	23.65	0.7013	24.92	0.7624	24.32	0.7351	24.46	0.7399
		0.01	23.33	0.6568	25.04	0.7694	24.01	0.6948	24.14	0.7105
	0.1	0.005	25.25	0.7654	25.99	0.8215	26.20	0.8178	26.31	0.8280
		0.01	25.47	0.7773	26.13	0.8252	26.26	0.8188	26.45	0.8336
	0.01	0.005	33.03	0.9599	35.40	0.9734	36.09	0.9739	35.59	0.9737
		0.01	33.05	0.9603	35.02	0.9721	35.53	0.9724	35.48	0.9724

Table 2. Removal of Gaussian + salt-and-pepper noise via the LATV- and pLATV-algorithm using approach 2 for the local bounds.

image	σ	s	LATV approach 2 with $\omega = 3$		pLATV approach 2 with $\omega = 3$	
			PSNR	MSSIM	PSNR	MSSIM
phantom	$\sqrt{0.02}$	0.005	25.77	0.9464	23.54	0.8608
		0.01	24.97	0.9431	23.05	0.8654
		0.1	0.005	27.94	0.9634	25.81
	0.1	0.01	27.03	0.9627	25.23	0.9166
		0.005	35.96	0.9957	32.27	0.9918
		0.01	32.89	0.9950	29.80	0.9885
cameraman	$\sqrt{0.02}$	0.005	25.78	0.7908	24.88	0.7585
		0.01	25.64	0.7932	24.47	0.7381
		0.1	0.005	27.34	0.8299	25.81
	0.1	0.01	27.27	0.8298	26.05	0.7926
		0.005	36.69	0.9607	32.91	0.9499
		0.01	35.49	0.9598	31.60	0.9420
cookies	$\sqrt{0.02}$	0.005	24.98	0.8032	24.42	0.7587
		0.01	24.89	0.8008	24.54	0.7761
		0.1	0.005	26.62	0.8481	26.25
	0.1	0.01	26.37	0.8413	26.00	0.8263
		0.005	38.16	0.9772	36.50	0.9774
		0.01	37.77	0.9793	36.06	0.9763

Table 3. Removal of Gaussian + random-valued impulse noise.

image	σ	r	$\alpha_1\alpha_2$ -PAPS		λ -pAPS		LATV approach 1 with $\omega = 11$		pLATV approach 1 with $\omega = 11$	
			PSNR	MSSIM	PSNR	MSSIM	PSNR	MSSIM	PSNR	MSSIM
phantom	$\sqrt{0.02}$	0.005	24.84	0.8988	24.92	0.8958	25.88	0.9234	24.99	0.8988
		0.01	24.13	0.8726	24.28	0.8701	25.32	0.9111	24.35	0.8738
	0.1	0.005	26.94	0.9228	26.94	0.9250	28.08	0.9417	27.02	0.9271
		0.01	25.94	0.8991	26.08	0.9092	27.42	0.9400	26.57	0.9245
	0.01	0.005	33.69	0.9919	31.61	0.9872	34.79	0.9929	33.08	0.9907
		0.01	30.55	0.9858	28.20	0.9725	32.43	0.9885	28.21	0.9726
cameraman	$\sqrt{0.02}$	0.005	25.13	0.7446	25.28	0.7465	25.65	0.7712	25.43	0.7619
		0.01	24.86	0.7271	25.15	0.7404	25.48	0.7609	25.27	0.7511
	0.1	0.005	26.35	0.7715	26.43	0.7792	27.00	0.8074	26.68	0.7943
		0.01	25.99	0.7533	26.13	0.7779	26.82	0.8027	26.32	0.7746
	0.01	0.005	33.39	0.9414	33.10	0.9412	35.52	0.9539	34.10	0.9520
		0.01	32.58	0.9383	32.58	0.9383	34.39	0.9496	32.53	0.9391
cookies	$\sqrt{0.02}$	0.005	24.27	0.7564	24.67	0.7724	24.74	0.7806	24.76	0.7780
		0.01	24.12	0.7475	24.63	0.7740	24.69	0.7758	24.64	0.7659
	0.1	0.005	25.65	0.8009	25.97	0.8191	26.14	0.8236	26.08	0.8164
		0.01	25.48	0.7960	25.71	0.8144	25.99	0.8208	25.95	0.8175
	0.01	0.005	36.01	0.9756	36.03	0.9758	37.21	0.9758	36.19	0.9759
		0.01	34.64	0.9692	35.60	0.9741	36.57	0.9740	35.74	0.9742

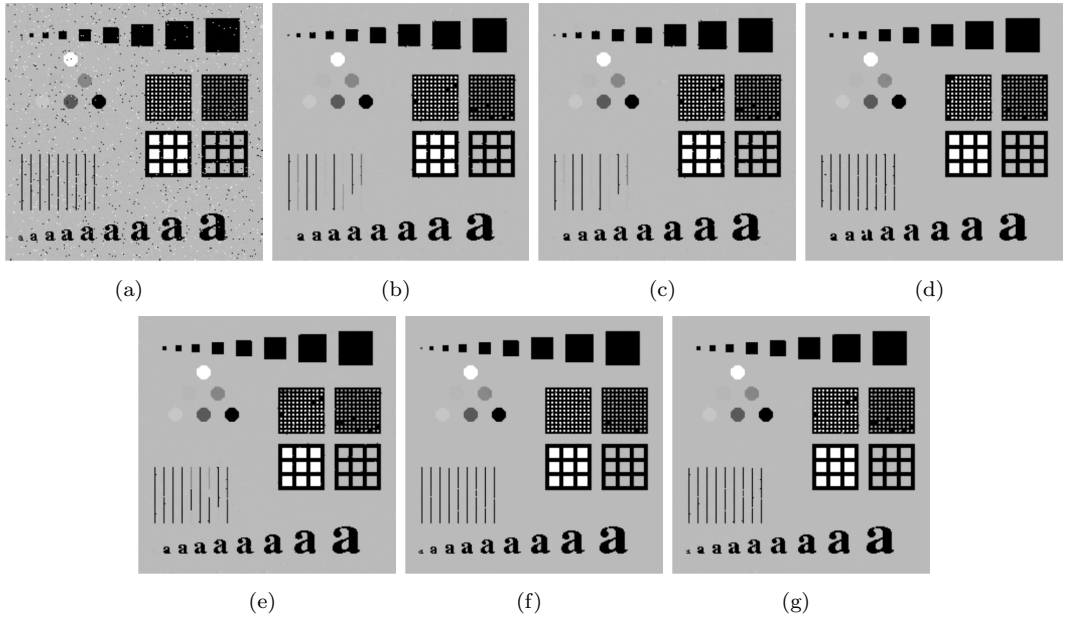


Figure 4. (a) Noisy image with $\sigma = 0.01$ and $s = 0.01$; (b) Restoration via $\alpha_1\text{-}\alpha_2\text{-}pAPS$; (c) Restoration via $\lambda\text{-}pAPS$; (d) Restoration via LATV approach 1; (e) Restoration via pLATV approach 1; (f) Restoration via LATV approach 2; (g) Restoration via pLATV approach 2.

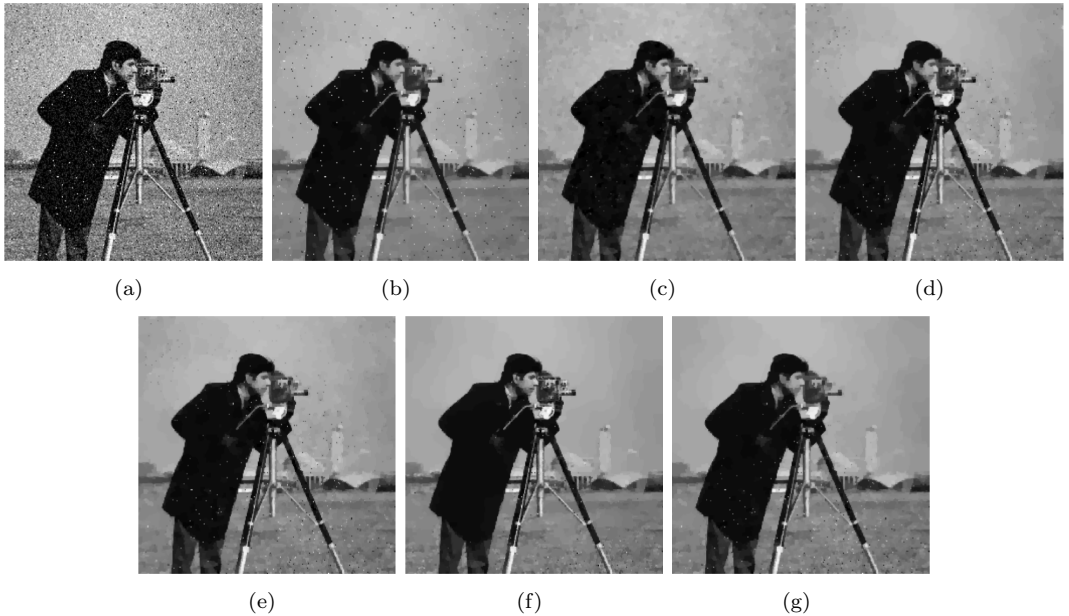


Figure 5. (a) Noisy image with $\sigma = 0.1$ and $s = 0.005$; (b) Restoration via $\alpha_1\text{-}\alpha_2\text{-}pAPS$; (c) Restoration via $\lambda\text{-}pAPS$; (d) Restoration via LATV approach 1; (e) Restoration via pLATV approach 1; (f) Restoration via LATV approach 2; (g) Restoration via pLATV approach 2.

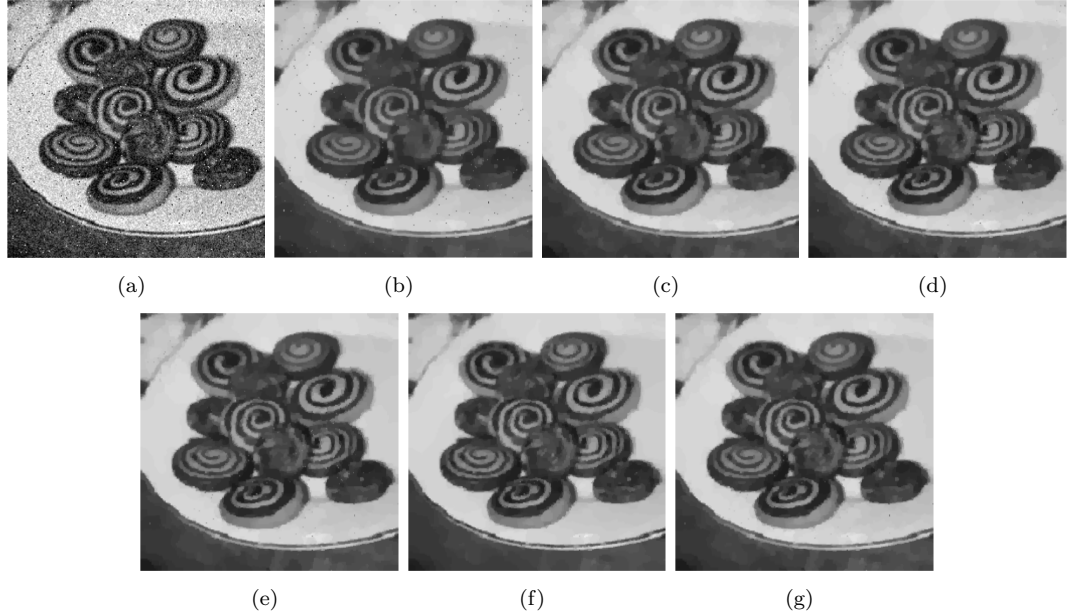


Figure 6. (a) Noisy image with $\sigma = 0.1$ and $s = 0.005$; (b) Restoration via α_1 - α_2 -pAPS; (c) Restoration via λ -pAPS; (d) Restoration via LATV; (e) Restoration via pLATV; (f) Restoration via LATV approach 2; (g) Restoration via pLATV approach 2.

Table 4. Removal of Gaussian + random-valued noise via the LATV- and pLATV-algorithm using approach 2.

image	σ	s	LATV approach 2 with $\omega = 3$		pLATV approach 2 with $\omega = 3$	
			PSNR	MSSIM	PSNR	MSSIM
phantom	$\sqrt{0.02}$	0.005	27.15	0.9555	26.05	0.9306
		0.01	26.57	0.9519	24.87	0.9001
	0.1	0.005	29.49	0.9678	28.79	0.9633
		0.01	28.74	0.9661	26.94	0.9309
	0.01	0.005	38.67	0.9973	35.30	0.9944
		0.01	35.74	0.9932	33.70	0.9931
cameraman	$\sqrt{0.02}$	0.005	26.01	0.7892	25.58	0.7761
		0.01	25.83	0.7826	25.38	0.7681
	0.1	0.005	27.39	0.8235	26.87	0.8092
		0.01	27.19	0.8191	26.67	0.8055
	0.01	0.005	36.00	0.9574	34.54	0.9559
		0.01	35.04	0.9549	33.84	0.9528
cookies	$\sqrt{0.02}$	0.005	25.25	0.8016	25.16	0.7995
		0.01	25.14	0.7984	24.95	0.7835
	0.1	0.005	26.71	0.8442	26.62	0.8418
		0.01	26.56	0.8425	26.51	0.8408
	0.01	0.005	37.72	0.9777	36.74	0.9779
		0.01	37.56	0.9782	36.47	0.9771

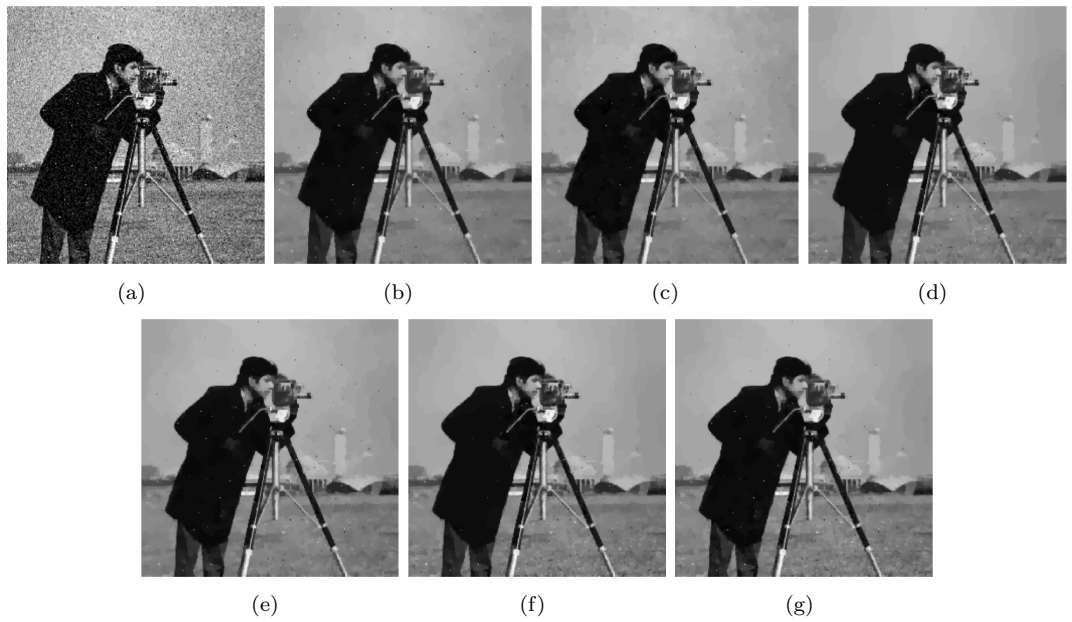


Figure 7. (a) Noisy image with $\sigma = 0.1$ and $r = 0.005$; (b) Restoration via α_1 - α_2 -pAPS; (c) Restoration via λ -pAPS; (d) Restoration via LATV approach 1; (e) Restoration via pLATV approach 1; (f) Restoration via LATV approach 2; (g) Restoration via pLATV approach 2

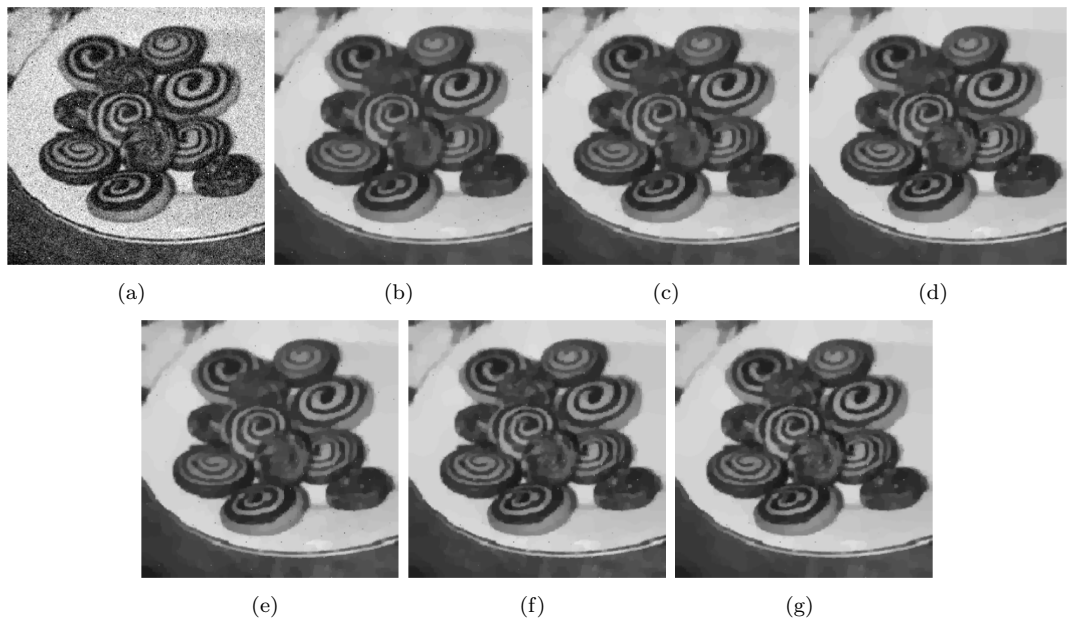


Figure 8. (a) Noisy image with $\sigma = 0.1$ and $r = 0.005$; (b) Restoration via α_1 - α_2 -pAPS; (c) Restoration via λ -pAPS; (d) Restoration via LATV approach 1; (e) Restoration via pLATV approach 1; (f) Restoration via LATV approach 2; (g) Restoration via pLATV approach 2.

We set $T_1 = \chi_{\Omega_1}$ and $T_2 = \chi_{\Omega_2}$ in (6). Since there is only one type of noise in Ω_1 and only one type of noise in Ω_2 , which is different to the noise in Ω_1 , the bound $B = \alpha_1\nu_1 + \alpha_2\nu_2$ in (7) does not seem reasonable anymore for all $x \in \Omega$. In particular, for approach 1 a better choice seems to choose B also spatially varying but not fully local as in approach 2. That is, in approach 1 we replace $B(u)$ by

$$B(u)(x) := \alpha_1\chi_{\Omega_1}(x)\nu_1(u) + \alpha_2\chi_{\Omega_2}(x)\nu_2(u),$$

where $\nu_1(u)$ is the EAV of salt-and-pepper noise and $\nu_2(u)$ is the variance of Gaussian noise, in our proposed locally adaptive total variation algorithms. For approach 2 we analogously set

$$B(u)(x) := c(\alpha_1\chi_{\Omega_1}(x)\nu_1(u)(x) + \alpha_2\chi_{\Omega_2}(x)\nu_2(u)(x)).$$

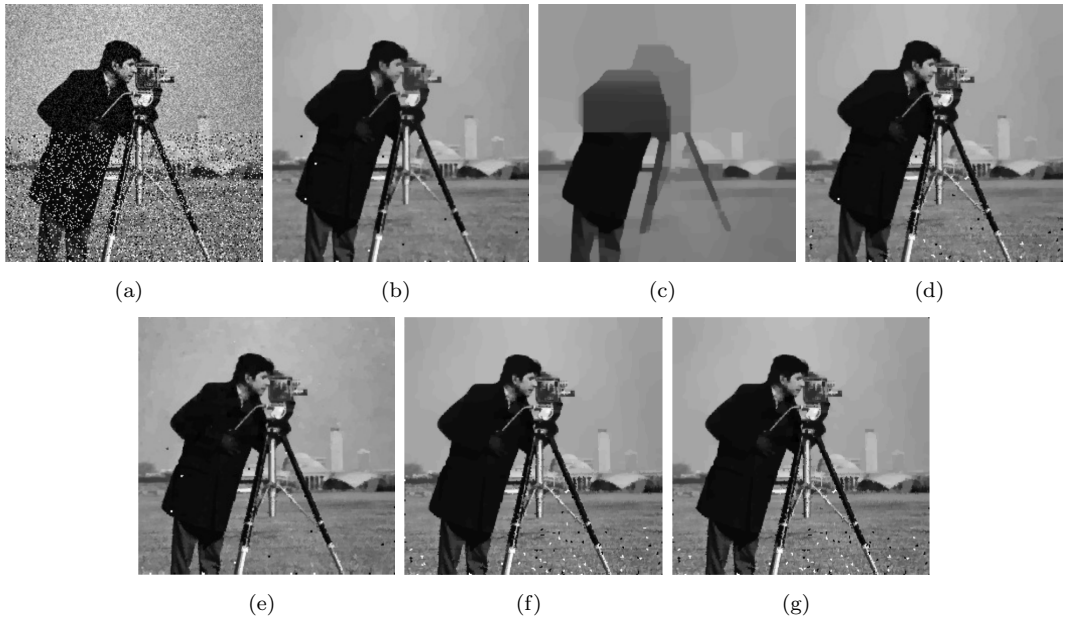


Figure 9. (a) Noisy image with $s = 0.1$ and $\sigma = 0.1$; (b) Restoration via α_1 - α_2 -pAPS (PSNR: 25.97; MSSIM: 0.8477); (c) Restoration via λ -pAPS (PSNR: 18.09; MSSIM: 0.6414); (d) Restoration via LATV approach 1 (PSNR: 25.74; MSSIM: 0.8609); (e) Restoration via pLATV approach 1 (PSNR: 26.41; MSSIM: 0.8609); (f) Restoration via LATV approach 2 (PSNR: 25.34; MSSIM 0.8687); (g) Restoration via pLATV approach 2 (PSNR: 25.26; MSSIM 0.8665).

In [28] it is demonstrated by using the α_1 - α_2 -pAPS, which chooses suitable parameters α_1 and α_2 , that the L^1 - L^2 -TV model is able to remove both types of noise considerably while preserving details at the same time from such images; see Figure 9(b). Using locally adaptive parameters this restoration capability can be improved; see Figure 9. In particular the pLATV-algorithm with approach 1 generates the best restoration with respect to PSNR, while the restoration obtained via the LATV-algorithm with approach 2 yields the largest MSSIM.

The λ -pAPS algorithm is clearly not suited to this task (see Figure 9(c)), since α_1 and α_2 are kept unchanged and λ is globally constant which makes it impossible to weight certain local parts of the image differently.

3.4. Non-homogeneous noise

We consider now an example, where the noise is non-homogeneously distributed over the image-domain. In particular, we look at the cameraman image degraded by salt-and-pepper noise with $s = 0.1$ and Gaussian white noise with variance $\sigma^2 = 0.01$ in the whole domain Ω except a rather small area $\tilde{\Omega}$ (highlighted in red in Figure 10(a)), where the variance of the Gaussian noise is 6 times larger, i.e., the variance $\tilde{\sigma}^2 = 0.06$ in this part. Since the noise is locally varying in this application, the bound B in approach 1 has to be adjusted to this situation. This is done by making ν_τ , $\tau = 1, 2$, locally dependent and we write $\nu_\tau = \nu_\tau(\hat{u})(x)$ to stress the dependency on the true image \hat{u} and on the localization $x \in \Omega$ in the image. Then $B(u)(x) = \alpha_1\nu_1(u)(x) + \alpha_2\nu_2(u)(x)$.

The results obtained by the λ -pAPS and LATV-algorithm using approach 1 and approach 2 are shown in Figure 10. We observe that the λ -pAPS-algorithm is neither able to remove the noise in $\tilde{\Omega}$ nor in the rest of the image. The LATV-algorithm with approach 1 is able to remove the noise in $\tilde{\Omega}$ considerably, but not the outliers in the rest of the image. A reason for this may be, that in this approach the values ν_1 and ν_2 may not be good approximations of the true values leading to an unreliable bound $B = \sum_{x \in \Omega} B(u)(x)$. On the contrary, if we use approach 2 and hence the true variance and EAV, then the LATV-algorithm generates a very satisfactory result, where all the noise seems to be removed, see Figure 10(d). This once more demonstrates that the choice of the local bounds is very crucial for the success of a locally varying regularization parameter method.

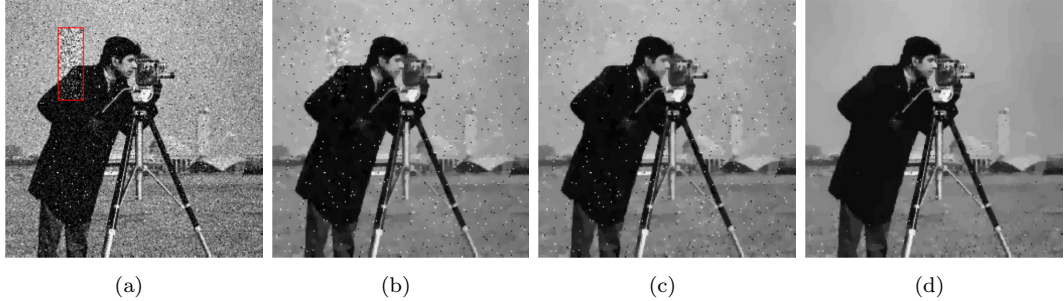


Figure 10. (a) Noisy image with $s = 0.005$, $\sigma = 0.1$, and $\sigma = \sqrt{0.06}$ in the highlighted area; (b) Restoration via λ -pAPS (PSNR: 22.33; MSSIM: 0.5886); (c) Restoration via LATV approach 1 (PSNR: 23.00; MSSIM: 0.6246); (d) Restoration via LATV approach 2 (PSNR: 26.24; MSSIM: 0.8065).

References

- [1] M. Alkämper and A. Langer, *Using DUNE-ACFem for non-smooth minimization of bounded variation functions*, Archive of Numerical Software 5 (2017), pp. 3–19.
- [2] A. Almansa, C. Ballester, V. Caselles, and G. Haro, *A TV based restoration model with local constraints*, J. Sci. Comput. 34 (2008), pp. 209–236. Available at <http://dx.doi.org/10.1007/s10915-007-9160-x>. MR 2377617 (2009d:94009)
- [3] L. Ambrosio, N. Fusco, and D. Pallara, *Functions of Bounded Variation and Free Discontinuity Problems*, Oxford Mathematical Monographs, The Clarendon Press, Oxford University Press, New York, 2000. MR 1857292 (2003a:49002)
- [4] M. Bertalmío, V. Caselles, B. Rougé, and A. Solé, *TV based image restoration with local constraints*, Journal of Scientific Computing 19 (2003), pp. 95–122.

- [5] A.C. Bovik, *Handbook of Image and Video Processing*, Academic press, 2010.
- [6] K. Bredies, K. Kunisch, and T. Pock, *Total generalized variation*, SIAM J. Imaging Sci. 3 (2010), pp. 492–526. Available at <http://dx.doi.org/10.1137/090769521>. MR 2736018 (2011k:49029)
- [7] J.F. Cai, R.H. Chan, and M. Nikolova, *Two-phase approach for deblurring images corrupted by impulse plus Gaussian noise*, Inverse Problems and Imaging 2 (2008), pp. 187–204.
- [8] L. Calatroni, J.C.D.L. Reyes, and C.B. Schönlieb, *Infimal convolution of data discrepancies for mixed noise removal*, SIAM Journal on Imaging Sciences 10 (2017), pp. 1196–1233.
- [9] V.C. Cao, J.C.D.L. Reyes, and C.B. Schönlieb, *Learning optimal spatially-dependent regularization parameters in total variation image restoration*, Inverse Problems 33 (2017), p. 074005.
- [10] A. Chambolle and T. Pock, *A first-order primal-dual algorithm for convex problems with applications to imaging*, Journal of Mathematical Imaging and Vision 40 (2011), pp. 120–145.
- [11] D.Q. Chen and L.Z. Cheng, *Spatially adapted regularization parameter selection based on the local discrepancy function for Poissonian image deblurring*, Inverse Problems 28 (2011), p. 015004.
- [12] J. Delon and A. Desolneux, *A patch-based approach for removing impulse or mixed Gaussian-impulse noise*, SIAM J. Imaging Sci. 6 (2013), pp. 1140–1174. Available at <http://dx.doi.org/10.1137/120885000>. MR 3071403
- [13] B. Dong, H. Ji, J. Li, Z. Shen, and Y. Xu, *Wavelet frame based blind image inpainting*, Applied and Computational Harmonic Analysis 32 (2012), pp. 268–279.
- [14] Y. Dong, M. Hintermüller, and M.M. Rincon-Camacho, *Automated regularization parameter selection in multi-scale total variation models for image restoration*, J. Math. Imaging Vision 40 (2011), pp. 82–104. Available at <http://dx.doi.org/10.1007/s10851-010-0248-9>. MR 2782120
- [15] R. Garnett, T. Huegerich, C. Chui, and W. He, *A universal noise removal algorithm with an impulse detector*, IEEE Transactions on Image Processing 14 (2005), pp. 1747–1754.
- [16] O. Ghita and P.F. Whelan, *A new GVF-based image enhancement formulation for use in the presence of mixed noise*, Pattern Recognition 43 (2010), pp. 2646–2658.
- [17] G. Gilboa, N. Sochen, and Y.Y. Zeevi, *Texture preserving variational denoising using an adaptive fidelity term*, in *Proc. VLsM*, Vol. 3. 2003.
- [18] E. Giusti, *Minimal Surfaces and Functions of Bounded Variation*, Monographs in Mathematics Vol. 80, Birkhäuser Verlag, Basel, 1984, Available at <http://dx.doi.org/10.1007/978-1-4684-9486-0>. MR 775682 (87a:58041)
- [19] Z. Gong, Z. Shen, and K.C. Toh, *Image restoration with mixed or unknown noises*, Multiscale Modeling & Simulation 12 (2014), pp. 458–487.
- [20] M. Hintermüller and A. Langer, *Subspace correction methods for a class of non-smooth and nonadditive convex variational problems with mixed L^1/L^2 data-fidelity in image processing*, SIAM J. Imaging Sci. 6 (2013), pp. 2134–2173. Available at <http://dx.doi.org/10.1137/120894130>. MR 3121758
- [21] M. Hintermüller and A. Langer, *Adaptive regularization for Parseval frames in image processing*, SFB-Report No. 2014-014 (2014), p. 12.
- [22] M. Hintermüller and A. Langer, *Non-overlapping domain decomposition methods for dual total variation based image denoising*, Journal of Scientific Computing 62 (2015), pp. 456–481.
- [23] M. Hintermüller and C.N. Rautenberg, *Optimal selection of the regularization function in a weighted total variation model. Part I: Modelling and theory*, Journal of Mathematical Imaging and Vision (2017), pp. 1–17.
- [24] M. Hintermüller, C.N. Rautenberg, T. Wu, and A. Langer, *Optimal selection of the regularization function in a weighted total variation model. Part II: Algorithm, its analysis and numerical tests*, Journal of Mathematical Imaging and Vision (2017), pp. 1–19.
- [25] M. Hintermüller and M.M. Rincon-Camacho, *Expected absolute value estimators for a*

- spatially adapted regularization parameter choice rule in L^1 -TV-based image restoration,* Inverse Problems 26 (2010), pp. 085005, 30. Available at <http://dx.doi.org/10.1088/0266-5611/26/8/085005>. MR 2658822 (2011d:65052)
- [26] Y.M. Huang, M.K. Ng, and Y.W. Wen, *Fast image restoration methods for impulse and Gaussian noises removal*, IEEE Signal Processing Letters 16 (2009), pp. 457–460.
 - [27] A. Langer, *Automated parameter selection for total variation minimization in image restoration*, Journal of Mathematical Imaging and Vision 57 (2017), pp. 239–268. Available at <http://dx.doi.org/10.1007/s10851-016-0676-2>.
 - [28] A. Langer, *Automated parameter selection in the L^1 - L^2 -TV model for removing Gaussian plus impulse noise*, Inverse Problems 33 (2017), p. 074002.
 - [29] B. Li, Q. Liu, J. Xu, and X. Luo, *A new method for removing mixed noises*, Science China Information Sciences 54 (2011), pp. 51–59.
 - [30] F. Li, M.K. Ng, and C. Shen, *Multiplicative noise removal with spatially varying regularization parameters*, SIAM J. Imaging Sci. 3 (2010), pp. 1–20. Available at <http://dx.doi.org/10.1137/090748421>. MR 2609456 (2011g:65066)
 - [31] F. Li and T. Zeng, *Image restoration via tight frame regularization and local constraints*, Journal of Scientific Computing 57 (2013), pp. 349–371.
 - [32] Y.R. Li, L. Shen, D.Q. Dai, and B.W. Suter, *Framelet algorithms for de-blurring images corrupted by impulse plus Gaussian noise*, IEEE Transactions on Image Processing 20 (2011), pp. 1822–1837.
 - [33] J. Liu, X.C. Tai, H. Huang, and Z. Huan, *A weighted dictionary learning model for denoising images corrupted by mixed noise*, IEEE Transactions on Image Processing 22 (2013), pp. 1108–1120.
 - [34] R.W. Liu, L. Shi, S.C.H. Yu, and D. Wang, *Box-constrained second-order total generalized variation minimization with a combined $L^{1,2}$ data-fidelity term for image reconstruction*, Journal of Electronic Imaging 24 (2015), pp. 033026–033026.
 - [35] E. López-Rubio, *Restoration of images corrupted by Gaussian and uniform impulsive noise*, Pattern Recognition 43 (2010), pp. 1835–1846.
 - [36] S. Peng and L. Lucke, *Fuzzy filtering for mixed noise removal during image processing*, in *Proceedings of the Third IEEE Conference on Fuzzy Systems, 1994. IEEE World Congress on Computational Intelligence*. IEEE, 1994, pp. 89–93.
 - [37] P. Rodríguez, R. Rojas, and B. Wohlberg, *Mixed Gaussian-impulse noise image restoration via total variation*, in *Acoustics, Speech and Signal Processing (ICASSP), 2012 IEEE International Conference on*. IEEE, 2012, pp. 1077–1080.
 - [38] Y. Shen, B. Han, and E. Braverman, *Removal of mixed Gaussian and impulse noise using directional tensor product complex tight framelets*, Journal of Mathematical Imaging and Vision (2015), pp. 1–14.
 - [39] D.M. Strong, P. Blomgren, and T.F. Chan, *Spatially adaptive local-feature-driven total variation minimizing image restoration*, in *Optical Science, Engineering and Instrumentation'97*. International Society for Optics and Photonics, 1997, pp. 222–233.
 - [40] Z. Wang, A.C. Bovik, H.R. Sheikh, and E.P. Simoncelli, *Image quality assessment: from error visibility to structural similarity*, IEEE Transactions on Image Processing 13 (2004), pp. 600–612.
 - [41] Y. Xiao, T. Zeng, J. Yu, and M.K. Ng, *Restoration of images corrupted by mixed Gaussian-impulse noise via l_1 - l_0 minimization*, Pattern Recognition 44 (2011), pp. 1708–1720.
 - [42] M. Yan, *Restoration of images corrupted by impulse noise and mixed Gaussian impulse noise using blind inpainting*, SIAM Journal on Imaging Sciences 6 (2013), pp. 1227–1245.
 - [43] J.X. Yang and H.R. Wu, *Mixed Gaussian and uniform impulse noise analysis using robust estimation for digital images*, in *16th International Conference on Digital Signal Processing, 2009*. IEEE, 2009, pp. 1–5.